Ocean Engineering 321 (2025) 120357

Contents lists available at ScienceDirect

Ocean Engineering

journal homepage: www.elsevier.com/locate/oceaneng

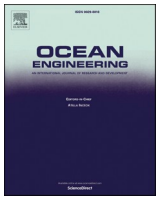

Research paper

Hull form optimisation to minimise the total resistance and dynamic responses of small fishing vessels

Muhammad Iqbal [a,b,*], Momchil Terziev [a], Tahsin Tezdogan [c], Atilla Incecik [a]

[a] Department of Naval Architecture, Ocean, and Marine Engineering, University of Strathclyde, Glasgow, G4 0LZ, UK
[b] Department of Naval Architecture, Diponegoro University, Semarang, 50275, Indonesia
[c] Department of Civil, Maritime and Environmental Engineering, University of Southampton, Southampton, UK

ARTICLE INFO

Keywords:
Small fishing vessel
KCS
GM ratio
Seakeeping
Response surface method
CFD

ABSTRACT

This paper presents a novel approach to ship hull form optimisation, aimed at minimising total resistance while simultaneously enhancing the seakeeping performance of a fishing vessel. When conducting optimisation process in minimising resistance, the method employs the minimisation of the y-axis radius of gyration (Ry) by optimising the longitudinal centre of gravity (LCG) and vertical centre of gravity (KG). The influence of altering LCG and KG on Ry, total resistance, and seakeeping is explored. Reducing Ry enhances seakeeping performance, lower added resistance, resulting in a reduced mean total resistance in waves. This finding demonstrates that it is possible to reduce resistance and improve seakeeping performance simultaneously without the need for multi-objective optimisation to balance the two. By employing the method outlined in this paper, seakeeping performance can be enhanced alongside resistance optimisation in a single process. The optimal hull form can reduce root mean square (RMS) vertical acceleration, RMS pitch motion, and added resistance on average by 1.79%, 1.51%, and 6.48%, respectively. In addition, the mean total resistance in waves for the optimised hull form was reduced by up to 4.15% compared to the initial hull form. This method offers a streamlined solution to achieving multiple performance objectives concurrently.

1. Introduction

Fishing at sea is the most dangerous occupation with a fatality rate for fishers is significantly higher than the national average in several countries (FAO, 2000). Fatal accidents in offshore fishing have multiple causes. For example, harsh environmental conditions, such as weather, operational area, season, and vessel characteristics being inherent to the nature of the work (Jin and Thunberg, 2005). In addition, human errors, including fatigue, multitasking, alcohol and drug use, and improper loading practices, can lead to collisions and sinkings (Ugurlu et al., 2020).

Environmental factors also influence the human factor that contributes to ship accidents, as stated in the study of Obeng et al. (2022). Wave-induced ship motions can undermine vessel stability, while also causing fatigue and seasickness among the crew, thereby impairing their performance and decision-making abilities. Small fishing vessels experience the highest fatality rates (Caamaño et al., 2018; Ugurlu et al., 2020; Wang et al., 2005), making research into the environmental impacts on these vessels crucial for enhancing the safety of this type of vessel.

Aside of the safety, it is essential to minimise the mean total resistance in waves to support decarbonisation efforts as recommended by the International Maritime Organization (IMO). The carbon intensity of international shipping is targeted to be reduced by at least 40% by 2030, compared to 2008 levels (IMO, 2018). Minimising total resistance not only reduces the carbon footprint of fishing vessels but also lowers fuel consumption. This reduction in fuel consumption can significantly lower operational costs for fishermen, ultimately benefiting them economically. Hydrodynamic optimisation is an effective way to enhance ship performance, by improving seakeeping performance or by minimising total resistance.

1.1. CoG optimisation

The loading conditions of fishing vessels change during operation. Optimisation in arranging and managing the centre of gravity (CoG) is essential for maintaining stability, improving seakeeping, ensuring overall safety, and reducing fuel consumption. This optimisation is

* Corresponding author. Department of Naval Architecture, Diponegoro University, Semarang, 50275, Indonesia.
E-mail address: muhammadiqbal@lecturer.undip.ac.id (M. Iqbal).

https://doi.org/10.1016/j.oceaneng.2025.120357
Received 3 September 2024; Received in revised form 25 December 2024; Accepted 9 January 2025
Available online 23 January 2025

similar to trim optimisation, which is one of the easiest and most cost-effective method for enhancing ship performance and reducing fuel consumption, as it does not alter the hull shape, or require retrofitting or energy-saving devices (Reichel et al., 2014).

Similar work related to managing CoG includes trim and ballast optimisation to minimise total resistance, as demonstrated by Reichel et al. (2014) and Hüffmeier et al. (2020). However, changes in trim conditions affect seakeeping and added resistance, as demonstrated by Shivachev et al. (2020) for the KCS model. Based on their investigation, motion responses increase slightly in the long wave region at larger trim angles. The added resistance trend is similar to that in calm water for short waves but differs in long waves. Trim by stern also affects ship stability, potentially increasing stability levels by 0.5%–5.4% (Wen and Fadillah, 2022) for tankers, container ships, and bulk carriers. Optimising the CoG for fishing vessels is a key focus of the present paper.

1.2. Hull form optimisation

In addition to CoG optimisation, the design of the vessel's hull form plays a significant role in its performance and must be considered in the early-stage design. An optimal hull form can improve resistance in both calm and in waves, as well as enhancing seakeeping behaviour, thereby improving safety. Hull form optimisation can be conducted globally (Bagheri et al., 2014) or locally, for example optimisation of the bow shape (Zhang et al., 2018) or stern shape (Rotteveel et al., 2017).

Optimising the hull form of fishing vessels to minimise total resistance can involve various scenarios, with each scenario's duration differing based on the time spent at sea. These scenarios include variations in displacement and speed (Tran et al., 2023; Zhao et al., 2021). However, one scenario, such as full load condition, can be used to optimise the hull form to minimise the resistance, improving the seakeeping and vessel stability, as demonstrated in Gammon (2011).

Unlike total resistance optimisation, which has a clear single objective function, seakeeping optimisation involves multiple objective functions that must be minimised. To address this complexity, Bales (1980) introduced an operability index in seakeeping optimisation for destroyer ships, combining various aspects such as pitch, roll, deck wetness, slamming, and acceleration into a single objective function. This approach was later adopted by Ozmen (1995) in the optimisation of seakeeping for fishing vessels. However, other researchers, including Grigoropoulos and Loukakis (1988), Gammon (2011), Bagheri et al. (2014) have opted to minimise each seakeeping performance parameter individually.

The optimisation of both calm water resistance and seakeeping is conducted simultaneously, streamlining the overall process and identified as a key contribution of this paper to the literature. The Response Surface Method (RSM) was selected as the optimisation technique, relying on gradient-based methods. The response surface is generated from a mathematical model obtained by regressing sample data from the Design of Experiments (DoE). Central Composite Design (CCD) with two variables was chosen as the DoE approach.

The present paper aims to optimise the FAO-01 fishing hull form by minimising the total resistance in calm water as the objective function. The Lackenby (1950) method was used to deform the initial hull form by varying the LCB and CB as design variables. The optimisation of CoG position is carried out by changing the LCG and KG for every hull from variation by minimising the radius gyration in y-axis (Ry) to enhance the seakeeping performance. The Ry introduced in this paper is a novel objective function in seakeeping optimisation to streamline the optimisation process.

2. Methodology

Fig. 1 illustrates the flowchart of the hull form optimisation process discussed in this paper. The study begins by identifying the subject ship and defining the simulation conditions. Following this, the research focuses on assessing the accuracy and numerical uncertainty of the CFD model. Once this foundation is established, two optimisation processes are undertaken.

The first optimisation involves altering the hull form by using the Lackenby (1950) method, which adjusts the longitudinal centre of buoyancy (LCB) and the block coefficient (CB). Combinations of LCB and CB are determined through a design of experimental approach, specifically using the Central Composite Design (CCD). Following the initial deformation, the hull form is further refined by optimising its centre of gravity, with adjustments made to the longitudinal centre of gravity

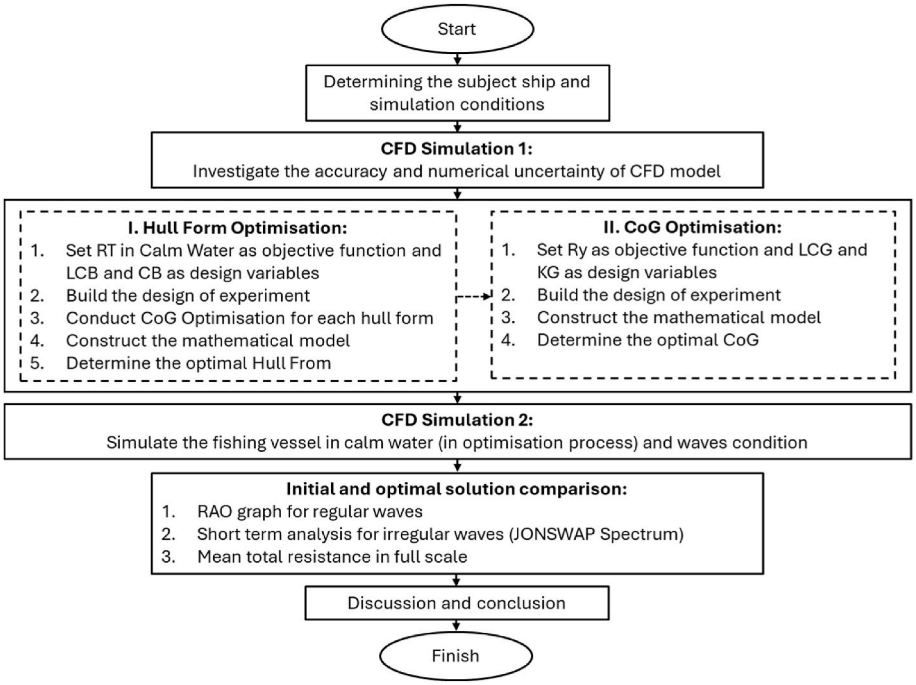

Fig. 1. Research flowchart.

(LCG) and the vertical centre of gravity (KG) to minimise the radius of gyration in y-axis (Ry).

To construct the mathematical model, the total resistance in calm water for each hull form variation is calculated using CFD simulations. This iterative process ultimately identifies the optimal hull form.

After determining the best hull form, the centre of gravity is further optimised to establish the optimal LCG and KG that minimise Ry. This optimisation results in a hull form with minimal resistance and enhanced dynamic performance. The study then conducts CFD simulations for both the original and optimised hull forms under calm water and wave conditions.

The final phase of the research compares the seakeeping performance and mean total resistance at full scale between the initial and optimised hull forms. The paper concludes with a discussion of the findings and final conclusions.

2.1. Case study ship and simulation conditions

This research focuses on a small fishing vessel FAO-01, detailed by Pérez-Arribas et al. (2022), including its lines plan and offset table data. The study by Pérez-Arribas et al. (2022) investigated the impact of adding a dihedral bulbous bow to the vessel to reduce its total resistance in calm water. Experimental data were scaled down by a factor of 1:4 to analyse and compare the resistance characteristics of the vessel, both with and without the dihedral bulbous bow. Complementary CFD simulations were later conducted by Díaz-Ojeda et al. (2023). The main dimensions of the FAO-01 vessel are listed in Table 1, while Fig. 2 showcases the 3D model derived from the referenced offset table.

Due to the lack of experimental data on the seakeeping performance of the FAO-01 vessel, this presented study relies on the KCS benchmark for seakeeping tests. These benchmarks were established by Simonsen et al. (2013) at a scale of 1:52.667 and by Shivachev et al. (2020) at a scale of 1:75, encompassing measurements of heave, pitch, and added resistance. The full-scale dimensions of the KCS are outlined in Table 2.

Simonsen et al. (2013) and Shivachev et al. (2020) conducted towing tank experiments on the KCS in head wave conditions, characterised by a wavelength of $\lambda/L_{bp} = 1.15$, a wave height of $H/\lambda = 1/60$, and a forward speed with a Froude number (Fr) of 0.26. Following the hull form optimisation process, additional CFD simulations, summarised in Table 3, were conducted to compare the seakeeping performance between the initial and optimised hull forms.

2.2. Optimisation process

2.2.1. Objective function and design variables

According to ITTC (2008), a service margin is incorporated into the required power calculated in calm water to account for the added resistance when a ship is operating in real-world sea and service conditions. Based on the traditional approach, this margin is approximately applied of 15–30% and the smaller ship requires more margin than the traditional estimation (Liu et al., 2019). Therefore, it is important to keep the total resistance in calm water as low as possible to reduce the mean total resistance in waves. This is achieved by setting calm water resistance as an objective function to be minimised by altering the LCB and CB as design variables to deform the hull form by using Lackenby Method. Table 4 presents the design variables and their corresponding codes for this scenario, where 0, 1, and −1 are codes represents initial, minimum, and maximum value of the actual design variables. The Longitudinal Centre of Buoyancy (LCB) is measured from the forward perpendicular (FP) as a percentage of the length between perpendiculars (L_{bp}).

Table 1
Main dimensions of FAO-01 fishing vessel.

Parameter	Value
Length overall, LOA (m)	9.232
Breadth moulded, B (m)	3.00
Depth moulded, D (m)	1.14
Loaded draft, T (m)	0.983
Volume Displacement, Δ(m^3)	5.846
Block coefficient, C_b (−)	0.267
Mid-boat section coefficient, Cm (−)	0.525
Wetted surface area, Aw (m^2)	23.914

However, the mean total resistance in waves consists of both the total resistance in calm water and the added resistance in waves. To ensure the added resistance is minimal, the vessel's dynamic response must be minimised due to the relationship between the added resistance and seakeeping performance. This is done by setting Ry as an objective function to be minimised for hull form variation and using LCG and KG as design variables. Minimising Ry also minimises the moment of inertia. Since the damping coefficient and added pitch moment of inertia remain unchanged (due to the same hull form) and the natural frequency changes only slightly, the pitch damping ratio increases. Consequently, the heave and pitch amplitudes are expected to decrease, allowing the seakeeping performance to be indirectly predicted and expediting the optimisation process in calm water resistance. Critically, obtaining an arrangement that satisfies the minimum Ry does not require any hydrodynamic calculations, as Ry is an intrinsic property of the vessel, which is a key advantage of the method. The best hull form is then expected to have minimum total resistance in waves and dynamic responses, resulting in better seakeeping performance.

2.2.2. Design of experiment (DoE)

Surrogate models are often utilised in engineering optimisation, which simplify complex systems using statistical techniques or regression (Xiaobo, 2017). These models link design variables to system responses, cutting down on the number of tests required to understand these relationships. Data for these models typically comes from Design of Experiments (DoE), random sampling, or experimental results (Guan et al., 2021). Once system responses like seakeeping performance are obtained, a statistical approach is used to build the mathematical model.

DoE systematically organises design variables and experiments, frequently employing fractional factorial experiments to test only a subset of possible combinations (Roy et al., 2008). For problems with fewer variables, methods like Central Composite Design (CCD) and Box-Behnken design are effective, especially for global hull form modifications (Lackenby, 1950). When dealing with numerous design variables, Latin Hypercube Sampling (LHS) is preferred.

This study's optimisation approach is grounded in Design of Experiments. Fig. 3 illustrates the use of Central Composite Design (CCD) for two design variables, where each variable is coded: 1 for the minimum value, 1 for the maximum, and 0 for the original model. The range between these values is ±5% of the original value. The additional code of ±1.414 represents fractional factorial designs, suited for two-level factorial experiments with two variables.

2.2.3. Approximate mathematical model

By using the Central Composite Design (CCD) method shown in Fig. 3, nine distinct design experiments are conducted, each yielding a specific result and is then used to develop a mathematical model, typically a quadratic polynomial. The regression equation for two variables is given in Eq. (1), where $y_i(x_j, x_k)$ represents the response or objective function influenced by the design variables x_j and x_k. In this context, the response (y_i) is associated with the total resistance in calm water, denoted as $RT(x_1, x_2)$.

$$y_i(x_j, x_k) = a + bx_j + cx_k + dx_j^2 + ex_k^2 + fx_jx_k \quad \text{Eq. 1}$$

2.2.4. Optimal solution

To accurately determine the minimum response, it is essential first to establish a mathematical equation for each response. The Response Surface Method (RSM) can produce one of three possible shapes: 1) a

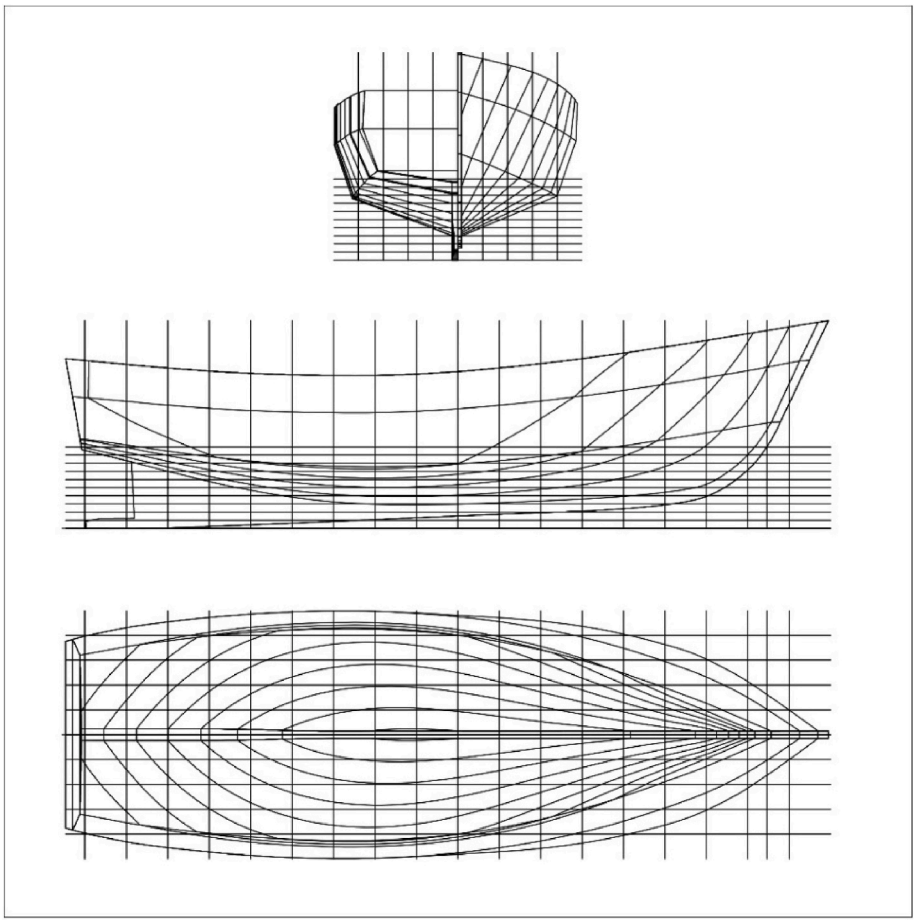

Fig. 2. Lines plan of subject ship (Pérez-Arribas et al., 2022).

Table 2
Main dimensions of KCS.

Dimensions	Value
Length between perpendicular, L_{bp} (m)	230
Breadth at water line, B (m)	32.2
Depth, D (m)	19.0
Loaded draft, T (m)	10.8
Block Coefficient	0.651

Table 3
Simulation condition in waves.

Parameter	Value
Scale Factor	4.00
Froude Number, Fr	0.33
Wavelength ratio, λ/Lbp	1.15 to 3.0
Wave steepness, H/λ	0.06

Table 4
Design variable and code for Transforming the hull form.

Design Variables	FAO-01		
	−1	0	1
LCB (%), x_1	51.196	53.890	56.585
CB (−), x_2	0.254	0.267	0.280

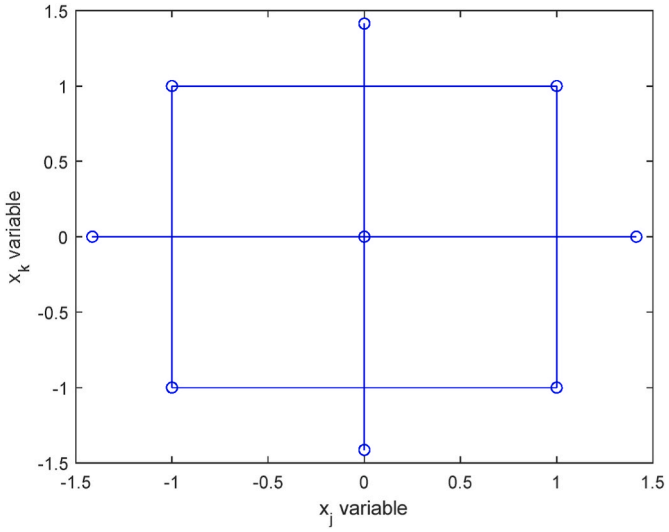

Fig. 3. Nine designs of experiment using central composite design (CCD).

Maximum, 2) a Minimum, or 3) a Saddle shape, where some of the response surfaces have a maximum and minimum value. The optimal solution is found by evaluating the first derivative of the response with respect to each variable (j,k), as shown in Eq. (2). This process requires solving two linear equations, each with two variables, to identify the stationary point (x_j, x_j). Constraints are necessary to ensure that the optimal solution remains feasible. In this study, the maximum and

minimum values for each variable are constrained to a range of ±2.5, corresponding to a ±12.5% deviation from the initial value.

$$y_{i\ max/min}(x_j, x_k) = \frac{dy_i(x_j, x_k)}{dx_j}\ y_{i\ max/min}(x_j, x_k) = \frac{dy_i(x_j, x_k)}{dx_k} \quad \text{Eq. 2}$$

2.3. CFD simulations

A fully non-linear Unsteady Reynolds-Averaged Navier-Stokes (URANS) approach is utilised in this study to incorporate the viscous effects into seakeeping simulations. Although this method is computationally intensive, it offers high accuracy. The numerical simulation methodology is described in detail, covering two scenarios: the calm water resistance and the seakeeping under head wave conditions. For the seakeeping simulations, the head waves are applied with two degrees of freedom—heave and pitch. The simulations are carried out using the Reynolds-Averaged Navier-Stokes (RANS) equations, which average out the effects of turbulence-induced velocity fluctuations. Siemens Star CCM + version 17.04, a commercial Computational Fluid Dynamics (CFD) software, is used to discretise the governing equations via the finite volume method (FVM). For unsteady problems, implicit methods with the first-order temporal discretisation are employed, while a second-order convection scheme is used for the convection term.

To handle the coupling between pressure and velocity, the Semi-Implicit Method for Pressure-Linked Equations (SIMPLE) algorithm is employed. Turbulence is modelled using the k-ε turbulence model, with the wall distance (y+) maintained between 30 and 100 to ensure accurate representation. The simulation also incorporates fifth-order waves for the seakeeping analysis, utilising the Volume of Fluid (VoF) method (Hirt and Nichols, 1981) to capture the free surface. Star CCM+ employs the High-Resolution Interface Capturing (HRIC) scheme based on the work by Muzaferija (1998) to maintain a sharp interface between phases.

Ship motions, including the heave and pitch, are modelled using the Dynamic Fluid Body Interaction (DFBI) module. The computational domain for the KCS model extends from −2.5 to 2.5 times the length overall (LOA) in length, −1.0 to 0.4 LOA in height, and 0 to 1.0 LOA in width, due to symmetry. The FAO-01 fishing boat's domain is adjusted for its unique dimensions, as illustrated in Fig. 4, spanning from −3.0 to 2.5 LOA in length, −1.5 to 1.0 LOA in height, and 0 to 1.5 LOA in width. The grid size, time step, and physics model determination methods are consistent across both models.

For calm water resistance and seakeeping simulations, symmetrical boundary conditions were enforced along the domain surface where the ship's centreline is located. All boundary surfaces within the computational domain were treated as velocity inlets, except the surface downstream of the vessel, which was designated as a pressure outlet. The hull surface itself was set as a no-slip boundary.

The Volume of Fluid (VoF) wave module was employed to define the initial velocities of both water and air in velocity inlet boundary, while the pressure outlet was set to maintain hydrostatic pressure. In resistance simulations, the wave damping was applied, whereas seakeeping simulations utilised the wave forcing to maintain the quality of wave according to as user set. These boundary conditions were positioned at a distance of 1LBP from both the inlet and outlet, and either 1.0 m or 0.3LBP from the side boundary for the KCS, with a distance of 0.5LBP for the fishing vessel model.

Star CCM+'s automatic meshing capabilities were used, applying the cartesian cut-cell method. The overset mesh approach used in this study allows focused mesh deformation on the hull, significantly reducing computational time compared to the moving mesh method, as reported by Mancini (2015) and Yulianti et al. (2022). The overset mesh divides the computational domain into two regions: background and overset.

In both regions, two specific areas were refined: the boundary layer and either the free surface (for seakeeping) or Kelvin wave zone (for calm water resistance). The height of the first boundary layer was calculated based on the target y + value, aimed between 30 and 100, appropriate for using the log-layer approach. Achieving the target y + involved determining the number of layers, as outlined by Terziev et al. (2022).

To refine the mesh in the Kelvin wake zone, the transverse wavelength (λ) was predicted using Eq. (3). This refinement zone extends 1L behind the vessel at an ingress angle of 20°. Here, k represents the wave number and g represents gravitational acceleration, and V represents the ship speed. This zone has an ingress angle of 20° and extends up to 1L behind the vessel.

$$\lambda = \frac{2\pi}{k} = \frac{2\pi}{(g/V^2)} \quad \text{Eq. 3}$$

To ensure accurate modelling of the Kelvin wake, the mesh is refined to include 24 cells per wavelength, which determines both the cell length and width. The height of the cells within this region is set to 1/8

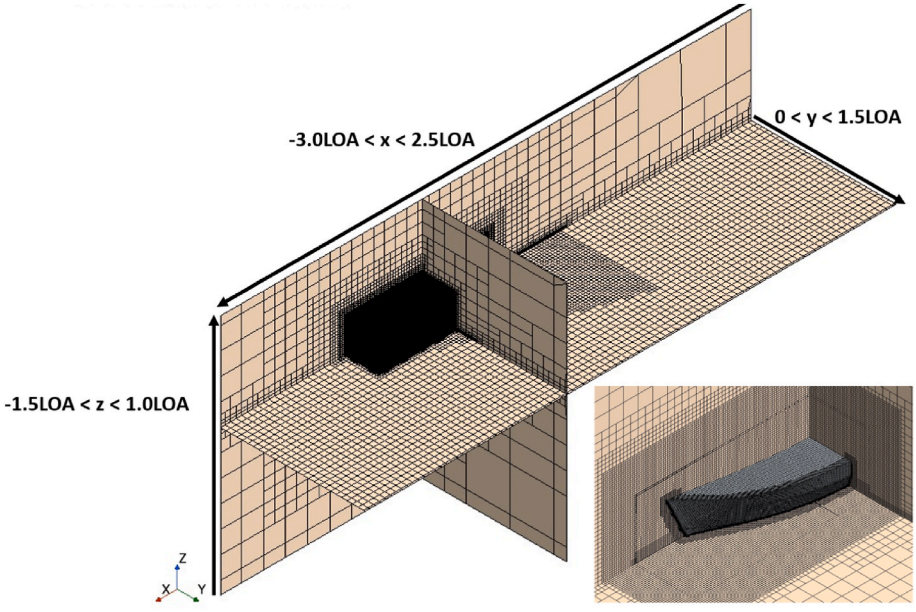

Fig. 4. Computational domain size and the result of mesh for Fishing Boat.

of the cell length in the x-direction. In the free surface region, cell dimensions are scaled by a factor of 2 relative to those in the Kelvin wake zone.

For the seakeeping simulations, the wavelength and wave height are predefined as input parameters to establish the wave environment. Following the guidelines set by the ITTC (2011), a minimum of 80 cells per wavelength and 20 cells per wave height are employed. The time step for calm water resistance simulations is calculated using a formula recommended by the ITTC (2014), shown in Eq. (4) which takes into account the ship's length (L) in metres and speed (V) in metres per second. For the time step in seakeeping analyses, the ITTC suggests a minimum time step of $T_e/100$, where T_e represents the wave encounter period. However, this study adopts a more refined approach, utilising a significantly smaller time step of $T_e/2^8$, as recommended by Cho et al. (2023), which provides enhanced accuracy beyond the ITTC's minimum requirement.

$$\Delta t = 0.005 - 0.01\,\frac{L}{V} \qquad \text{Eq. 4}$$

3. Results and discussion

3.1. Accuracy and numerical uncertainty of the CFD model

Table 5 presents a comparison between the results obtained from the CFD model and the experimental data, serving as a basis for assessing the accuracy of the CFD simulations. The study includes both calm waters, represented by the coefficient of total resistance ($CT*10^3$), and wave conditions, represented by transfer function (TF) that relates the wave to resulting responses of the ship. In calm water, the total resistance coefficient was analysed, revealing that the CFD results differ from the experimental references by approximately 1%.

Under wave conditions, the heave TF shows a minor discrepancy of 0.43% when compared to the experimental data, reflecting a high level of accuracy. However, the pitch TF displays a slightly larger variance, with a difference of 4.89% from the experimental results. Despite this larger gap, the accuracy is still considered within an acceptable range, as it remains under the 5% threshold.

For the added resistance TF in wave conditions, the CFD results were compared against two different sets of experimental data. When compared with the findings of Simonsen et al. (2013), the CFD results show a difference of 5.03%. Meanwhile, a comparison with the data from Shivachev et al. (2020) reveals a variance of −6.21%. Although these differences are slightly larger, they remain within a reasonable range for practical applications, validating the reliability of the CFD model for predicting both resistance and seakeeping characteristics.

Given that the accuracy study of the KCS model exhibited strong alignment with the Experimental Fluid Dynamics (EFD) results, the same CFD modelling was applied to simulate the FAO-01 fishing vessel. Table 6 compares the CFD predictions with experimental data for the FAO-01 vessel's total resistance in calm water at a Froude number of 0.33, showing that the CFD result deviates by only −0.97% from the experimental findings, indicating excellent accuracy.

Table 6
The results comparison between present CFD and experimental data of FAO-01 Fishing Boat at Fr = 0.33.

	RT (N)
EFD (Díaz-Ojeda et al., 2023)	15.31
Present CFD	15.162
Difference (%)	**−0.97%**

The CFD setup used in this study is referred to as the fine configuration. To assess numerical uncertainty, a refinement factor of $\sqrt{2}$ was applied to create a medium configuration for the KCS model, while a factor of 1.23 was used for the FAO-01 fishing vessel. This medium configuration was then further coarsened by the same factor for the KCS model and by 1.24 for the FAO-01 vessel. The results obtained from the Grid Convergence Index (GCI) based on Roache (1998). Table 7 presents the numerical uncertainty for the KCS model, with results below 5%. Similarly, Table 8 shows that the numerical uncertainty for the total resistance of the FAO-01 fishing vessel in calm water was generally below 5%.

3.2. Optimisation in CoG position of the parent hull form

Before undertaking hull form optimisation according to Fig. 1, this subsection will examine the relationship between changes in the centre of gravity (CoG) position, the radius of gyration in the y-direction (Ry), and the total resistance in calm water (RT_{calm}). This analysis is conducted by performing a design of experiments (DoE), as outlined in Table 9, and by developing mathematical models and response surfaces for each objective function. The calm water resistance was predicted using CFD simulations. The resulting Ry and RT_{calm} for each loading condition based on the DoE are also presented in Table 9. It should be noted that the initial LCG was determined based on the LCB location in the no-trim condition, while KG was determined as 75% of KM. Then, the optimal location can be achieved after the optimisation process.

$$Ry\,(m) = 0.5533 - 0.0002x_1 + 0.0016x_2 + 0.0020{x_1}^2 + 0.0003{x_2}^2 \qquad \text{Eq. 5}$$

$$RT\,(N) = 15.162 - 0.0746x_1 - 0.0161x_2 + 0.1282{x_1}^2 + 0.0042{x_2}^2 + 0.0132x_1x_2 \qquad \text{Eq. 6}$$

The mathematical models for the Ry and RT_{calm} responses are presented in Eq. (5) and Eq. (6), respectively. The corresponding response

Table 5
The results comparison between present CFD and experimental data of the KCS at Fr = 0.26

	Calm Water	Wave Condition (λ/Lbp = 1.15)		
	CT $*10^3$ $\left(\frac{RT_{calm}\,(N)}{0.5\rho V^2 S\,(N)}\right)$	Heave TF $\left(\frac{z_a\,(m)}{\zeta\,(m)}\right)$	Pitch TF $\left(\frac{\theta_a\,(rad)}{k\zeta\,(rad)}\right)$	Added Resistance TF $\left(\frac{Mean\,RT_{wave} - RT_{calm}\,(N)}{\rho g\zeta^2 (B^2/L)\,(N)}\right)$
EFD (Simonsen et al., 2013)	4.31	0.950	0.693	9.106
Present CFD	4.36	0.954	0.727	9.564
Difference (%)	**1.06%**	**0.43%**	**4.89%**	**5.03%**
EFD (Shivachev et al., 2020)	4.41	–	–	9.78
Present CFD	4.36	0.941	0.735	9.173
Difference (%)	**−1.23%**	**-**	**-**	**−6.21%**

Table 7
Numerical uncertainty results for the KCS.

	Calm Water	Wave Condition (λ/Lbp = 1.15)		
	CT *10^3 $\left(\frac{RT_{calm}\,(N)}{0.5\rho V^2 S\,(N)}\right)$	Heave TF $\left(\frac{z_a\,(m)}{\zeta\,(m)}\right)$	Pitch TF $\left(\frac{\theta_a\,(rad)}{k\zeta\,(rad)}\right)$	Added Resistance TF $\left(\frac{Mean\,RT_{wave}-RT_{calm}\,(N)}{\rho g\zeta^2(B^2/L)\,(N)}\right)$
Fine Configuration	total cell = 3,591,024, time step = 0.01845 s	total cell = 4,330,069, time step = 0.00360 s		
Medium Configuration	total cell = 1,396,929, time step = 0.02609 s	total cell = 1,889,342, time step = 0.00509 s		
Coarse Configuration	total cell = 561,609, time step = 0.03690 s	total cell = 923,707, time step = 0.00720 s		
Fine solution, S_1	4.36	0.9541	0.7269	9.5638
Medium solution, S_2	4.44	0.9550	0.7265	9.8579
Coarse solution, S_3	4.58	0.9650	0.7131	15.2748
Medium-Fine, ε_{21}	0.8	0.0009	−0.0004	0.2941
Coarse-Medium, ε_{32}	1.4	0.0100	−0.0134	5.4169
Convergence ratio, R	0.57143	0.0900	0.0299	0.0543
Order of accuracy, p	1.61471	6.9479	10.1322	8.4062
GCI Method (%)	**3.05810**	**0.0117**	**0.0021**	**0.2207**

Table 8
Numerical uncertainty results for FAO-01 fishing vessel.

	RT Calm Water	Wave Condition (λ/Lbp = 1.5)		
		Heave TF $\left(\frac{z_a\,(m)}{\zeta\,(m)}\right)$	Pitch TF $\left(\frac{\theta_a\,(rad)}{k\zeta\,(rad)}\right)$	Added Resistance TF $\left(\frac{Mean\,RT_{wave}-RT_{calm}\,(N)}{\rho g\zeta^2(B^2/L)\,(N)}\right)$
Fine Configuration	total cells = 1,715,717, time step = 0.0131 s	total cell = 3,536,648, time step = 0.0026 s		
Medium Configuration	total cells = 1,010,918, time step = 0.0161 s	total cell = 1,419,264, time step = 0.0037 s		
Coarse Configuration	total cells = 577,607, time step = 0.0200 s	total cell = 512,760, time step = 0.0052 s		
Fine solution, S_1	15.1616 N	1.1177	0.6884	1.9716
Medium solution, S_2	15.5010 N	1.1157	0.6837	1.9473
Coarse solution, S_3	16.2236 N	1.0937	0.6657	1.8631
Medium-Fine, ε_{21}	0.33939	−0.00200	−0.0047	−0.0243
Coarse-Medium, ε_{32}	0.72260	−0.02200	−0.0180	−0.0842
Convergence ratio, R	0.46969	0.09091	0.2611	0.2886
Order of accuracy, p	3.39085	6.91886	3.8745	3.5857
GCI Method (%)	**2.7495**	**0.0224**	**0.3016**	**0.6250**

Table 9
Responses of Ry and RT with LCG and KG variation.

Loading Condition	X_1 (−)	X_2 (−)	LCG (m)	KG (m)	R_y (m)	RT CFD (N)
Initial	0	0	0.945	0.379	0.5533	15.162
LC 1	1	1	0.992	0.398	0.5570	15.225
LC 2	1	−1	0.992	0.360	0.5539	15.253
LC 3	−1	1	0.898	0.398	0.5575	15.316
LC 4	−1	−1	0.898	0.360	0.5543	15.397
LC 5	−1.414	0	0.878	0.379	0.5577	15.543
LC 6	1.414	0	1.012	0.379	0.5570	15.287
LC 7	0	−1.414	0.945	0.352	0.5517	15.174
LC 8	0	1.414	0.945	0.406	0.5563	15.160

surfaces are illustrated in Fig. 5. The robustness of these mathematical models is demonstrated in Fig. 6. According to Abdulkadir et al. (2021), a mathematical model is considered to yield good results if the predicted and actual data align closely with the fitted line, y = x, represented by the black line in Fig. 6. As shown in Fig. 6-a, the R^2 value for the Ry response is high at 0.9998, indicating a close match between the predicted and actual values. In contrast, on Fig. 6-b, the R^2 value for the total resistance in calm water is slightly lower at 0.9757. This suggests that, according to this model, the longitudinal centre of gravity (LCG) and the vertical centre of gravity (KG) account for 97.57% of the total resistance of FAO-01, with the remaining 2.43% attributed to other, unidentified factors.

The initial positions of the longitudinal centre of gravity (LCG) and the vertical centre of gravity (KG), along with their optimal positions for minimising Ry and RT_{calm} based on the equations, are also presented in Fig. 5 and Table 10. The total resistance results predicted by Eq. (6) are

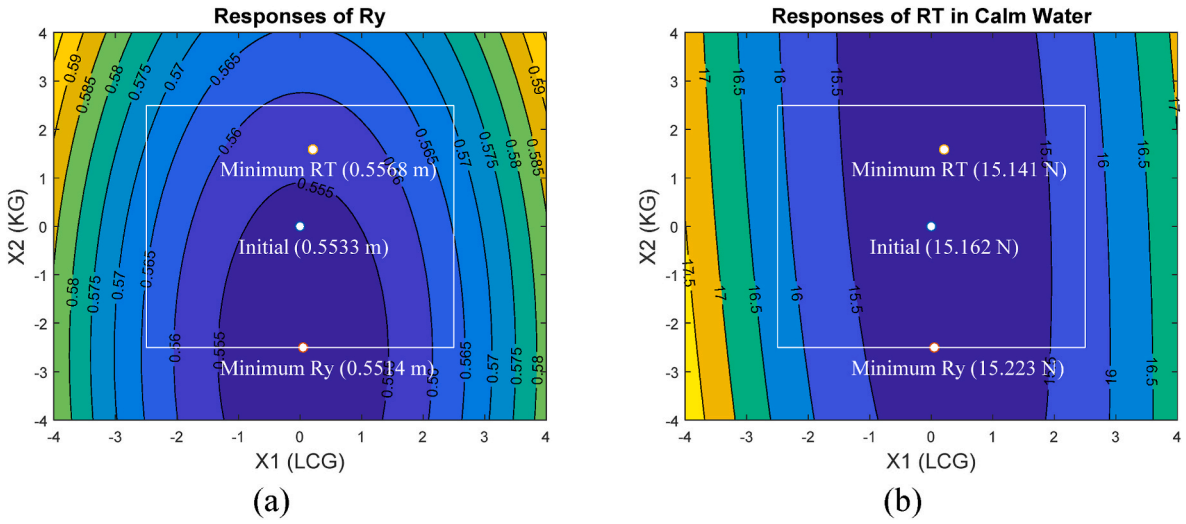

Fig. 5. Response Surface Result for Ry (left) and RT_{calm} (right) Influenced by LCG and KG with the constrains and optimal location.

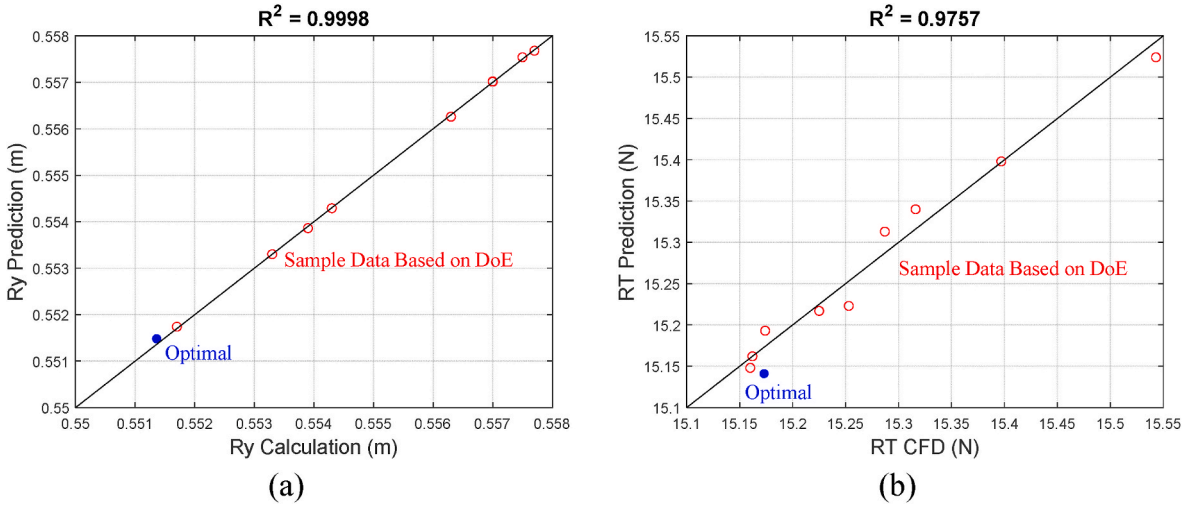

Fig. 6. The Comparison between Actual and Predicted Ry and RT values.

Table 10
The RT comparison.

Loading Condition	x_1 (−)	x_2 (−)	LCG (m)	KG (m)	RT CFD (N)	RT Eq. 6 (N)
Initial	0.00	0.00	0.945	0.379	15.162	15.162
Minimum Ry	0.050	−2.50	0.947	0.332	15.165	15.223
Minimum RT	0.209	1.588	0.955	0.409	15.173	15.141
Minimimum Ry and Initial Difference (%)					**0.020%**	**0.402%**
Minimimum RT and Initial Difference (%)					**0.073%**	**−0.136%**

compared with the actual results obtained from CFD simulations. It is shown that optimising the CoG for minimal Ry leads to an increase in the total resistance in calm water by up to 0.402% according to Eq. (6), and by 0.02% based on CFD simulations. Conversely, optimising the CoG for minimal RT results in a reduction in the total resistance by up to 0.136%, according to Eq. (6), and an increase of up to 0.073% based on CFD simulations.

These findings suggest that minimising the Ry value has a negligible impact on total resistance in calm water, as the differences between the optimal CoG for Ry, the initial condition, and the optimal CoG for RT, are not significant. On the other hand, reducing Ry improves seakeeping performance. Therefore, by minimising the Ry value, dynamic responses can be reduced while total resistance remains largely unchanged.

Fig. 7 illustrates the comparison of free surface elevation on the hull between the experimental test conducted by Pérez-Arribas et al. (2022), the initial loading condition (LC), the optimal LC for minimal Ry, and the optimal LC for minimal RT based on CFD simulations. Visually, there is no noticeable difference between CFD simulation results. All wave elevation on hull based on CFD is similar to experimental test too. However, the resulting trim varies across the three different LCs. As the optimal LCs for Ry and RT shift forward towards the bow, the trim by bow increases, depending on how far the loading condition has been adjusted, as described in Table 10.

Fig. 8 provides a quantitative comparison of the free surface elevation on the hull for the three different LCs. It can be observed that the elevations are similar, with no significant differences. Both Figs. 7 and 8 confirm that the lack of a significant difference in total resistance results in the same trend for the free surface elevations across the three different LCs.

3.3. *Hull form optimisation*

After ensuring that determining the best location for LCG and KG with minimal Ry does not significantly affect total resistance in calm water, the research in this paper is continued by applying the research

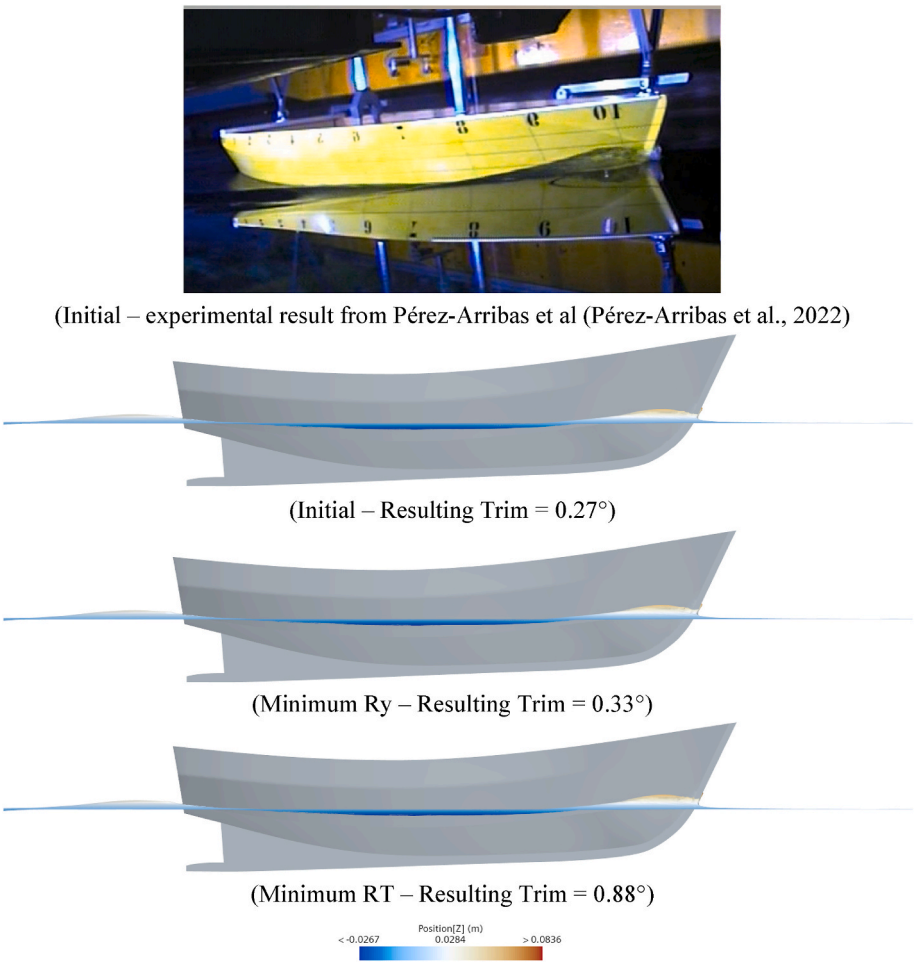

Fig. 7. The visualisation of free surface elevation on hull.

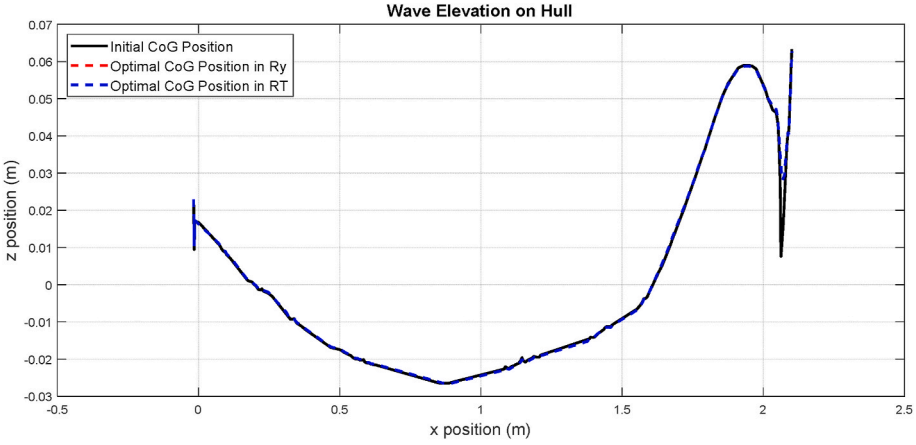

Fig. 8. Comparison of Free Surface Elevation on the Hull between different CoG Position.

flowchart, shown in Fig. 1. The percentage of Longitudinal Centre of Buoyancy (LCB) and block coefficient (CB) were used to deform an initial hull form by using the Lackenby method (Lackenby, 1950).

$$RT\,(N) = 15.162 - 0.326x_1 + 0.49x_2 + 0.647{x_1}^2 + 0.216{x_2}^2 + 0.294x_1x_2 \quad \text{Eq. 7}$$

Table 11 shows the results of nine combinations of LCB and CB based on central composite design to develop new hull form with the CFD results for total resistance in calm water. During the simulation, the position of LCG and KG for each hull form was obtained from the CoG optimisation step by minimising Ry with changes in LCG and KG. The resulted mathematical model based on Table 11 is shown in Eq. (7). The visualisation of the response surfaces is shown in Fig. 9-a and the plot of the actual RT based on CFD versus the predicted RT based on Eq. (7) is presented in Fig. 9-b. The R^2 value of Eq. (7) is 0.9936, which is sufficiently high, explaining the relationship between LCB and CB to the total resistance in calm water. This is evidenced by the plot of actual versus

Table 11
Responses of RT with LCB and CB variations.

Hull Form	X_1	X_2	LCB (%)	CB (−)	RT CFD (N)
Initial	0	0	53.890	0.267	15.162
Hull Form −1	1	1	56.585	0.280	16.472
Hull Form −2	1	−1	56.585	0.254	14.871
Hull Form −3	−1	1	51.196	0.280	16.641
Hull Form −4	−1	−1	51.196	0.254	16.216
Hull Form −5	−1.414	0	50.079	0.267	16.817
Hull Form −6	1.414	0	57.701	0.267	16.041
Hull Form −7	0	−1.414	53.890	0.248	14.898
Hull Form −8	0	1.414	53.890	0.286	16.238

predicted values, where both results align closely.

Fig. 10 presents a comparison of the lines plan between the initial and optimal hull forms in terms of calm water resistance (RT). The optimal hull form has an increased LCB percentage, measured from FP, resulting in the LCB shifting towards the stern. It should be noted that the total displacement is kept constant by maintaining the same length and draft. Consequently, the breadth of the fishing vessel has been adjusted, increasing from 0.678 m to 0.732 m.

As explained earlier, after generating various hull forms during the design of experiments step, the location of the LCG and KG for each hull form was determined by conducting CoG optimisation to minimise Ry. Then, the CFD simulation in calm water resistance could be carried out. The same procedure was repeated after identifying the hull form with the minimal resistance. Table 12 shows the comparison of the LCG and KG locations between the initial and optimal results.

Once the optimal hull form with the optimal loading condition has been determined, CFD simulations in calm water and in waves can be carried out. Table 13 shows the results of the total resistance in calm water for the optimal hull form in RT and compares it with the initial hull form. Based on Eq. (7), the optimal hull form can reduce the total resistance by up to 3.15%. However, the results from the CFD simulations show a reduction of 2.92%. The difference between the predicted and actual results is small, at −0.24%.

The optimal hull form in RT shifted the LCB towards the stern. Then, the bow shape region became smaller (sharper), making the hull entrance angle lower. These conditions make the pressure force become lower than the initial hull form, as shown in Fig. 11. The free surface elevation on the hull surface also reduced in bow region as illustrated in

Table 12
The comparison initial and optimal loading conditions for optimal hull form.

Loading Condition	LCG (m)	KG (m)	R_y
Initial	0.908	0.415	0.5559
Optimal	0.929	0.363	0.5506
Difference (%)			**−0.95%**

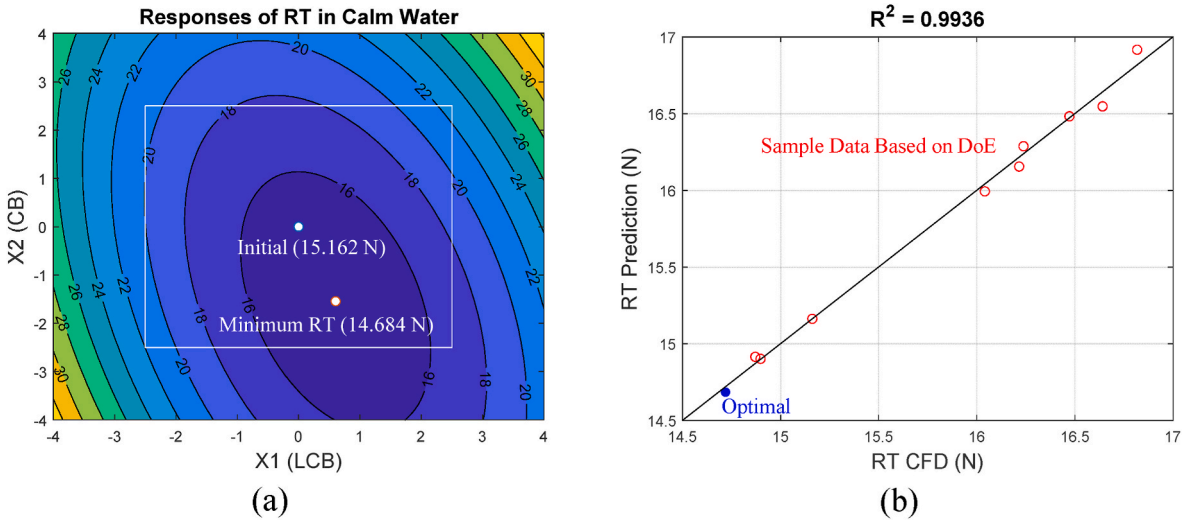

Fig. 9. The Comparison of Response Surface Result for RT Influenced by LCB and CB with the constrains

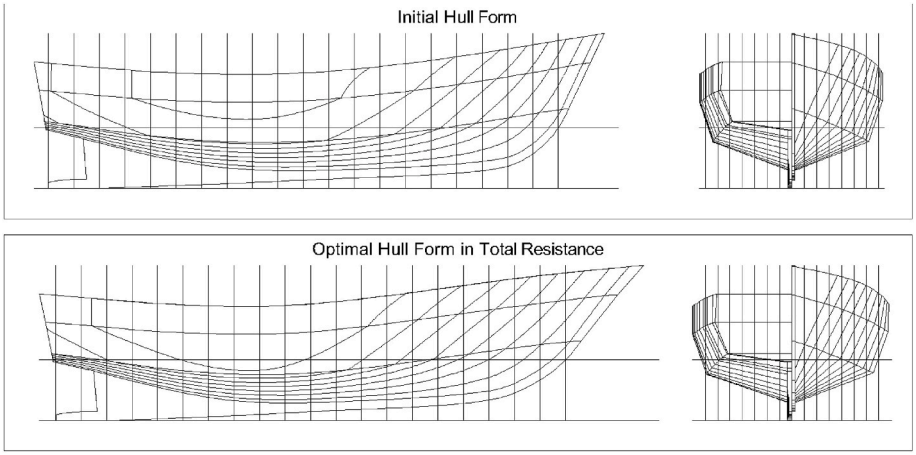

Fig. 10. Hull form comparison between initial (a) and optimal (b).

Table 13
The RT comparison between Equation and CFD.

Hull Form	x_1	x_2	LCB (%)	CB (−)	RT CFD (N)	RT Eq. 7 (N)	Difference (%)
Initial	0.00	0.00	53.820	0.267	15.162	15.162	0
Optimal	0.604	−1.545	55.517	0.246	14.719	14.684	−0.24
Difference (%)					**−2.92**	**−3.15**	

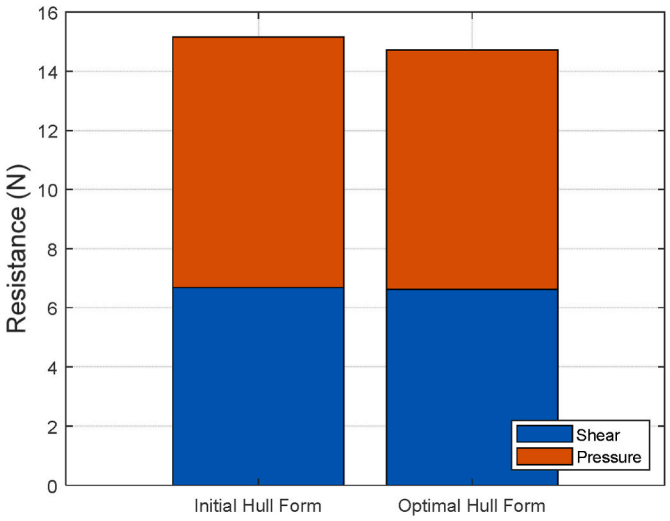

Fig. 11. The comparison of total resistance Decomposition between initial and optimal hull form.

Figs. 12 and 13. The optimal hull form results in trim by bow higher than the initial one, from 0.27° to 1.14°.

3.4. Results of seakeeping performance in regular waves

After predicting the total resistance in calm water, the CFD simulations in waves can be carried out. Fig. 14 compares the mean total resistance in waves (RT) of the initial hull form and the optimal hull form. The figure also provides the calm water resistance result for each hull form. The added resistance is calculated by subtracting the total resistance in calm water from the mean total resistance in waves. It can be observed that the optimal hull form in total resistance in calm water exhibits the highest RT in waves at the first two lower wavelength ratio. However, when the wavelength ratio exceeds 1.5, the optimal hull form exhibits lower mean RT in waves than the initial hull form.

Table 14 and Fig. 15 jointly show the Response Amplitude Operator (RAO) of heave and pitch motions, as well as the added resistance, comparing the initial hull form with the optimal hull form for minimal total resistance in calm water (RT). The trends for three RAOs are similar to the mean total resistance in waves. For the first two low wavelength ratios (1.15 and 1.5), the RAO values of the optimal hull form are higher than those of the initial hull form, while the last three wavelength ratios also show higher values for the optimal hull form. However, the pitch RAO value for the optimal hull form at a wavelength ratio of 2 is not significantly different from the initial hull form results (1.101 versus 1.105). Although all RAOs of the optimal hull form are higher than the initial hull form in the first two low wavelengths, the differences are not as significant as those observed in the last three wavelength ratios, making the performance of the optimal hull form better than that of the initial hull form.

3.5. Results of seakeeping performance in irregular waves

The comparison between two RAOs does not provide information on the percentage by which the optimal hull form can reduce heave, pitch, and added resistance relative to the initial hull form. To obtain this information, the RAOs must be combined with the wave spectra that represent the specific location of the vessel. There is a potential for wave periods to closely match the vessel's natural period, leading to resonance conditions that result in high response amplitudes.

In this subsection, a short-term seakeeping analysis is conducted by combining the RAO with the wave spectrum representing the operational area of the fishing vessels. The JONSWAP spectrum with $\gamma = 2.5$ (Eq. (8)) was employed to characterise the Java Sea, which serves as the operational area for this vessel (Djatmiko, 2012). Using Eq. (9), the response spectrum was then determined. Subsequently, the n-th moment calculation in Eq. (10) was used to determine the displacement (motion), velocity, and acceleration spectra. Finally, the RMS value for the response was calculated using Eq. (11).

Given that the fishing boat is assumed to operate in the Java Sea, Indonesia, a wave scatter diagram representative of this area is required. However, not all combinations of peak periods (Tp) and significant wave heights (Hs) are considered. This study focuses on the three most frequently occurring Tp and Hs combinations to evaluate their impact on the fishing boat's responses. Table 15 displays a partial wave scatter

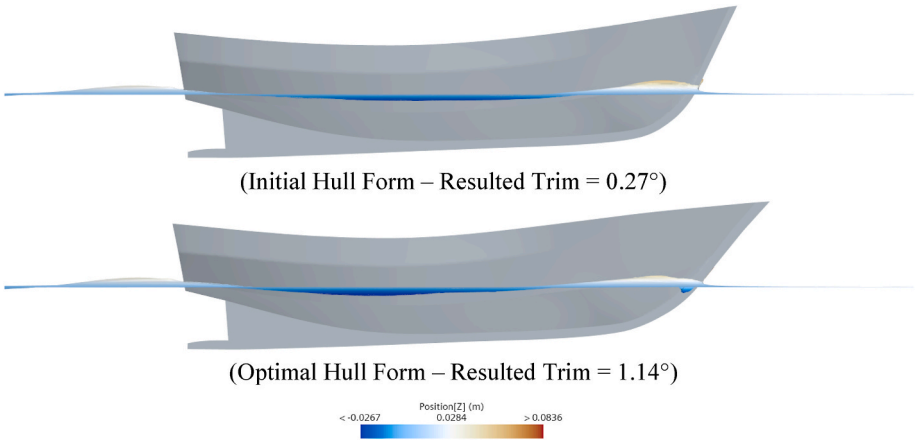

Fig. 12. Result of CFD resistance simulation at Fr = 0.33.

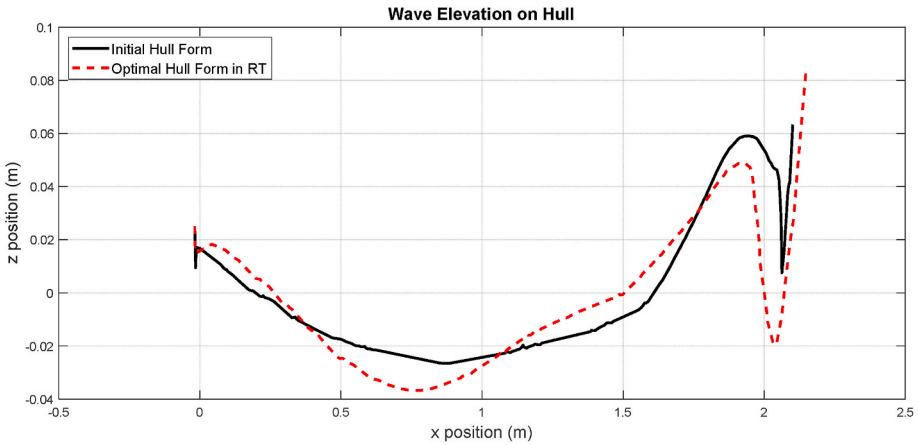

Fig. 13. Comparison of Wave Elevation on the Hull between different Hull Form.

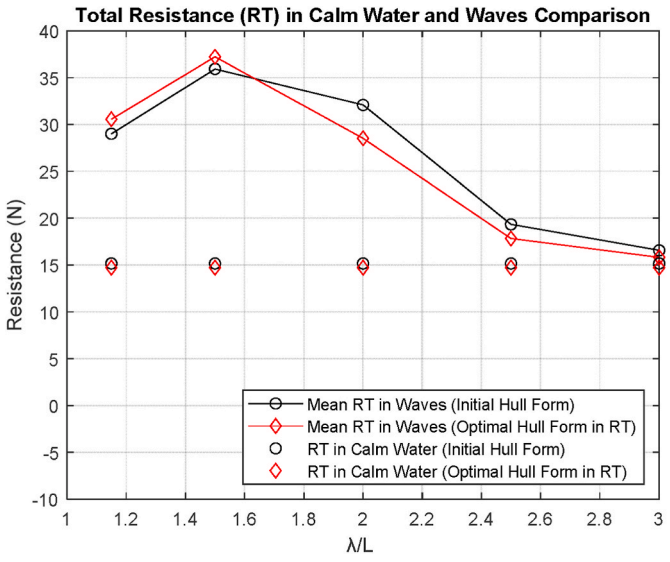

Fig. 14. Total resistance in calm water and mean total resistance in waves.

Table 14
Response amplitude Operator comparison.

λ/L	Initial			Optimal Hull Form in RT		
	Heave TF	Pitch TF	C_{AW}	Heave TF	Pitch TF	C_{AW}
1.15	0.320	0.225	1.035	0.351	0.253	1.185
1.5	0.917	0.570	1.553	0.956	0.617	1.682
2	1.387	1.105	1.265	1.299	1.101	1.032
2.5	1.069	1.153	0.312	1.034	1.073	0.232
3	0.983	1.075	0.105	0.959	1.016	0.082

diagram of the Java Sea, emphasising the conditions with the highest occurrence. The selected Hs-Tp combinations in Table 15 represent 89.2% of the recorded conditions in the Java Sea over the course of a year.

$$S_\zeta(\omega) = \left[\frac{\alpha g^2}{\omega^5} exp\left\{-\frac{5}{4}\left(\frac{\omega_p}{\omega}\right)^{-4}\right\}\right]\gamma^{exp\left\{-\frac{(\omega-\omega_p)^2}{2\sigma^2\omega_p^2}\right\}} \quad \text{Eq. 8}$$

$$S_r(\omega) = RAO^2 \times S_\zeta(\omega) \quad \text{Eq. 9}$$

$$m_n = \int_0^\infty \omega^n S_r(\omega) d\omega \quad \text{Eq. 10}$$

$$RMS = \sqrt{m_n} \quad \text{Eq. 11}$$

The RAOs of the fishing vessel, initially obtained at model scale, were subsequently scaled up to full scale since the wave scatter data in this study reflects actual (full-scale) conditions. It is assumed that the scaling of all responses follows a linear relationship. Spline interpolation was applied to generate data between the five wavelength ratios used in the CFD simulations for determining the RAOs.

One criterion for evaluating the vertical motion of the fishing vessel in the working area is the vertical acceleration. Given the small size of the fishing vessel in this study, it is assumed that most fishermen work near the centre of the ship. As a result, the effect of longitudinal distance from the centre of gravity on the vertical acceleration due to pitch is disregarded, and only heave is considered when calculating vertical acceleration. This criterion is assessed using the RMS value ($\sqrt{m_4}$).

The RMS values of vertical acceleration, expressed in g units, are presented in Table 16. The criterion for acceptable vertical acceleration is that accelerations should remain below 0.2 g. The results show that not all Tp-Hs combinations meet this criterion. The significant wave height (Hs) of 1.25 m is identified as the worst case for heave acceleration, as the RMS vertical acceleration exceeds the limit at Tp = 0.35 s. Overall, the optimal hull form can reduce heave accelerations by an average of 1.79%.

The seakeeping criterion for the pitch motions in this study is based on the RMS pitch motion ($\sqrt{m_0}$), with a threshold set at 3°. Therefore, the spectral analysis for pitch is presented in terms of motion responses. Table 17 compares the RMS pitch responses between the initial and optimised hull forms. The findings reveal that, similar to the RMS vertical acceleration, the difference in RMS pitch response is significantly influenced by the peak period (Tp), whereas the significant wave height (Hs) has little to no effect on the variation. The optimised hull form achieves an average reduction of 1.51% in RMS pitch response.

The final assessment of seakeeping performance in irregular waves, as depicted in Table 18, focuses on the mean added resistance. Although there is no specific criterion established for the added resistance, the results for mean added resistance ($2m_0$) under the optimal loading condition were evaluated based on their reduction relative to the initial hull form. The influence of Hs and Tp on mean added resistance is consistent with the trends observed in the heave and pitch response analysis. The optimised hull form results in an average reduction of 6.48% in the mean added resistance.

Fig. 16 shows the comparison of the percentage reduction in RMS vertical acceleration, RMS pitch, and mean added resistance for the optimised hull form compared to the initial hull form. The added resistance exhibits the greatest reduction among these metrics. This reduction is particularly significant as the added resistance directly impacts fuel consumption and overall operational efficiency. The

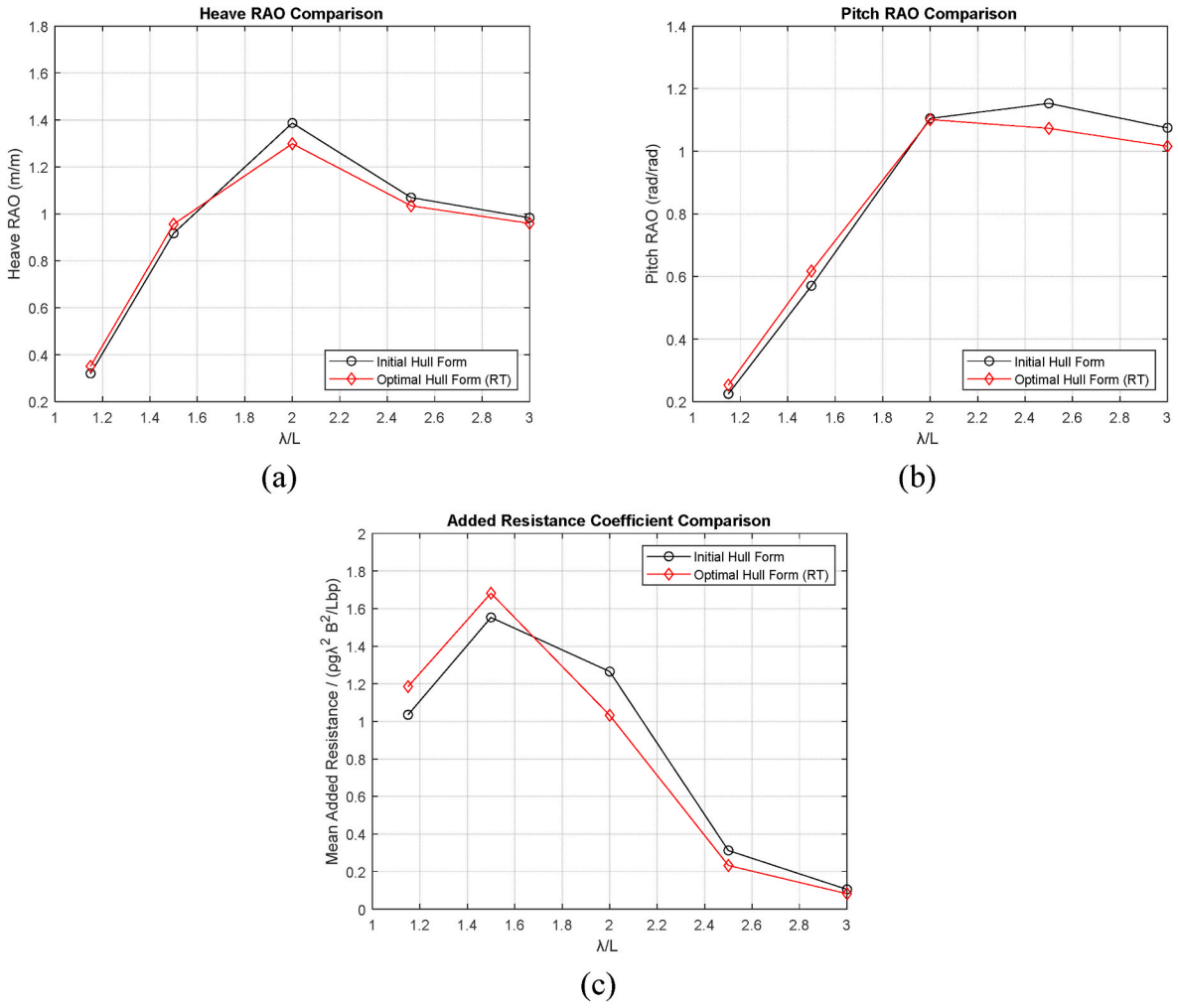

Fig. 15. Heave, pitch RAO and added resistance coefficient comparison.

Table 15
The highest occurrence of Tp and Hs in Java Seas, Indonesia.

Hs (m) \ Tp (s)	3–4	4–5	5–6
0.0–0.5	23.99%	7.30%	0.49%
0.5–1.0	11.27%	27.17%	6.43%
1.0–1.5	0.00%	2.52%	10.03%

findings suggest that the optimised hull form not only improves seakeeping performance but also offers potential benefits in terms of reducing fuel costs and minimising the environmental footprint of the vessel during operations. The actual benefits due to reducing in resistance can be seen after determining the mean total resistance in waves in the following subchapter.

3.6. The comparison of mean total resistance in full scale

Based on the finding in subsection 3.2, the same hull form with optimal loading conditions in Ry does not significantly affect the total resistance, as the location of optimal loading condition for Ry and for calm water total resistance is quite similar. However, the added resistance in waves can lead to markedly different mean total resistance results. Thus, in addition to assessing seakeeping performance, it is essential to calculate the total resistance in waves after modifying the hull form for both seakeeping and resistance optimisations.

Total resistance in waves is decomposed into the total resistance in calm water and the mean added resistance in waves. The added resistance at full scale has already been calculated during the seakeeping assessment in the previous subchapter. Therefore, it is necessary to determine the total resistance in calm water for each hull form variation. In this study, the Froude method is employed to extrapolate the total

Table 16
The comparison of RMS Vertical Acceleration ($\sqrt{m_4}$) in g unit and its reduction.

	Tp (s)								
	3.5	4.5	5.5	3.5	4.5	5.5	3.5	4.5	5.5
Hs (m)	Initial			Optimum Hull Form in RT			Difference		
0.25	0.056	0.036	0.027	0.055	0.036	0.026	−2.09%	−1.52%	−1.75%
0.75	0.168	0.109	0.080	0.164	0.108	0.078	−2.09%	−1.52%	−1.75%
1.25	0.279	0.182	0.133	0.273	0.179	0.130	−2.09%	−1.52%	−1.75%
Average							**−1.79%**		

Table 17
The comparison of RMS Pitch Response ($\sqrt{m_0}$) in degree.

	Tp (s)								
	3.5	4.5	5.5	3.5	4.5	5.5	3.5	4.5	5.5
Hs (m)	Original			Optimum Hull Form in RT			Difference		
0.25	1.013	0.665	0.490	0.999	0.655	0.482	−1.31%	−1.48%	−1.73%
0.75	3.038	1.994	1.471	2.998	1.964	1.446	−1.31%	−1.48%	−1.73%
1.25	5.063	3.323	2.452	4.997	3.274	2.410	−1.31%	−1.48%	−1.73%
Average							**−1.51%**		

Table 18
The comparison of mean added resistance in kilo Newton.

	Tp (s)								
	3.5	4.5	5.5	3.5	4.5	5.5	3.5	4.5	5.5
Hs (m)	Initial			Optimum Hull Form in RT			Difference		
0.25	0.049	0.020	0.011	0.045	0.019	0.010	−7.35%	−5.61%	−6.47%
0.75	0.437	0.184	0.096	0.405	0.173	0.090	−7.35%	−5.61%	−6.47%
1.25	1.214	0.510	0.267	1.125	0.481	0.250	−7.35%	−5.61%	−6.47%
Average							**−6.48%**		

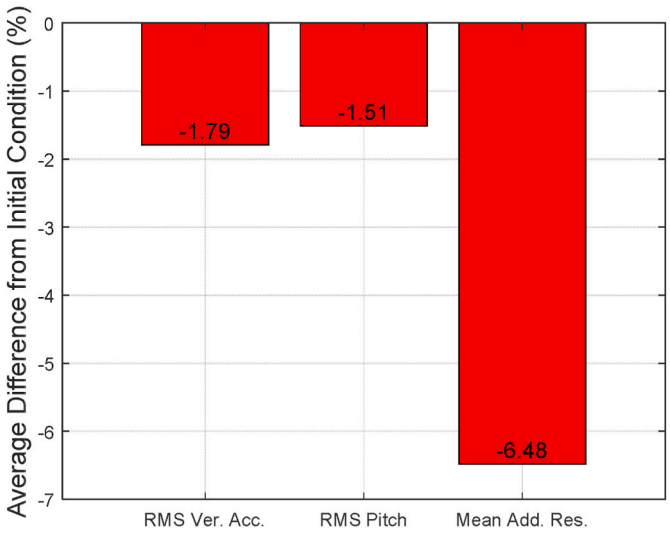

Fig. 16. The comparison of seakeeping performance.

resistance in calm water from the model scale results.

The power of the initial hull form taken from Pérez-Arribas et al. (2022) lies between 2 and 4 kW (there is no specific value from the paper). The power of the initial hull form from the present study is 2.603 kW, as shown in Table 19, which is similar to Pérez-Arribas et al. (2022).

The reduction for the optimal hull form in RT compared to the initial hull form is 3.47%. This achievement is lower than the additional dihedral bulbous bow, which can reduce resistance by up to 5%. However, the findings from this paper show that the optimisation of the hull form in RT was successful, reducing the power close to the results achieved with the additional dihedral bulbous bow with improvement in seakeeping performance. Further investigation should be undertaken at higher speeds for a comprehensive comparison.

Table 20 presents the full scale of the mean total resistance in regular waves for each optimal solution compared to the initial condition across different H_s and T_p combinations. The optimal hull form in calm water total resistance shifted the LCB to stern, results in an average reduction of 4.15% of mean total resistance. Since the total resistance in calm water between the initial and optimal loading conditions shows no significant difference, added resistance plays a crucial role in determining the total resistance in waves. The optimal loading condition can reduce the added resistance, thereby lowering the total resistance in waves.

This finding demonstrates that it is possible to reduce the resistance and improve seakeeping performance simultaneously without the need for multi-objective optimisation to balance the two. By employing the method outlined in this paper, seakeeping performance can be enhanced alongside resistance optimisation in a single process. This integrated approach simplifies the design process, allowing for the development of hull forms that are both efficient in terms of resistance and effective in seakeeping performance in various sea conditions. Consequently, the vessel benefits from enhanced safety, while also potentially reducing fuel consumption and lowering environmental impact. This method offers a streamlined solution to achieving multiple performance objectives concurrently.

4. Conclusions

The hull form optimisation aimed at minimising the calm water resistance and the dynamic responses of small fishing vessels has been successfully achieved simultaneously. During the optimisation process, calm water resistance was directly targeted, while seakeeping performance was indirectly considered, thereby accelerating the optimisation.

Table 19
The comparison of calm water total resistance in full scale (kN).

Hull Form	Model				Full Scale			
	RT (N)	CT $*10^3$	CF $*10^3$	Cr $*10^3$	CF $*10^3$	CT $*10^3$	RT (kN)	Power (kW)
Initial	15.162	8.563	3.670	4.894	2.549	7.443	0.8434	2.603
Opt. HF in RT	14.719	8.252	3.670	4.583	2.549	7.132	0.8141	2.512
Difference (%)								**−3.47**

Table 20
The comparison of the mean total resistance in full scale (kN).

	Tp (s)								
	3.5	4.5	5.5	3.5	4.5	5.5	3.5	4.5	5.5
Hs (m)	Initial			Optimum HF in RT			Difference		
0.25	0.892	0.864	0.854	0.859	0.833	0.824	−3.68%	−3.52%	−3.51%
0.75	1.281	1.027	0.940	1.219	0.987	0.904	−4.80%	−3.86%	−3.78%
1.25	2.058	1.353	1.110	1.939	1.296	1.064	−5.76%	−4.28%	−4.20%
Average							**−4.15%**		

The optimal longitudinal and vertical centres of gravity (LCG and KG) were determined by minimising the y-axis radius of gyration (Ry) while optimising the hull form in calm water. Reducing Ry is expected to decrease pitch response, resulting in a hull form with minimal resistance and dynamic responses.

Calm water total resistance was predicted using CFD simulations, but CFD was not employed during the seakeeping optimisation process, helping to reduce computational costs. Once the optimal hull form with minimal calm water total resistance and Ry was identified, its seakeeping performance in regular waves was evaluated using CFD simulations and compared to the initial hull form. The Response Amplitude Operator (RAO) was generated for five different wave-to-ship length ratios. To assess the seakeeping performance of the optimal hull form in irregular waves, a spectral technique analysis was conducted using the most common significant wave height (Hs) and peak period (Tp) conditions in the Java Sea, Indonesia.

The results indicate that the optimal hull form can reduce RMS vertical acceleration, RMS pitch motion, and added resistance by an average of 1.79%, 1.51%, and 6.48%, respectively. When combining calm water total resistance with added resistance at full scale, the mean total resistance in waves for the optimised hull form was reduced by up to 4.15% compared to the initial hull form. This finding demonstrates that resistance can be reduced, and seakeeping performance can be enhanced simultaneously, eliminating the need for multi-objective optimisation to balance these two aspects in this study.

CRediT authorship contribution statement

Muhammad Iqbal: Writing – original draft, Methodology. **Momchil Terziev:** Writing – review & editing, Supervision, Software. **Tahsin Tezdogan:** Writing – review & editing, Supervision. **Atilla Incecik:** Writing – review & editing, Supervision.

Declaration of competing interest

The authors declare that they have no known competing financial interests or personal relationships that could have appeared to influence the work reported in this paper.

Acknowledgement

Results were obtained using the ARCHIE-WeSt High-Performance Computer (www.archie-west.ac.uk) based at the University of Strathclyde. The work published in this paper is drawn from the first author's PhD thesis. The first author gratefully acknowledges Diponegoro University in Indonesia for giving him a PhD scholarship to support his study at the University of Strathclyde, Glasgow.

References

Abdulkadir, I., Mohammed, B.S., Liew, M.S., Wahab, M.M.A., 2021. Modelling and multi-objective optimization of the fresh and mechanical properties of self-compacting high volume fly ash ECC (HVFA-ECC) using response surface methodology (RSM). Case Stud. Constr. Mater. 14, e00525.

Bagheri, L., Ghassemi, H., Dehghanian, A., 2014. Optimizing the seakeeping performance of ship hull forms using genetic algorithm. TransNav Int. J. Mar. Navig. Saf. Sea Transp. 8, 49–57.

Bales, N.K., 1980. Optimizing the seakeeping performance of destroyer type hulls. In: Published by: David W. Taylor Naval Ship Research \& Development Center, Ship Performance Department, Bethesda, Maryland, USA. Prepared for the 13th Symposium on Naval Hydrodynamics, ONR, Tokyo, Japan, 1980.

Caamaño, L.S., González, M.M., Casás, V.D., 2018. On the feasibility of a real time stability assessment for fishing vessels. Ocean Eng 159, 76–87.

Cho, J.-H., Lee, S.-H., Oh, D., Paik, K.-J., 2023. A numerical study on the added resistance and motion of a ship in bow quartering waves using a soft spring system. Ocean Eng 280, 114620.

Díaz-Ojeda, H.R., Pérez-Arribas, F., Turnock, S.R., 2023. The influence of dihedral bulbous bows on the resistance of small fishing vessels: a numerical study. Ocean Eng 281, 114661.

Djatmiko, E.B., 2012. Behavior and operability of marine Buildings on random waves. Indonesian). ITS-Press. Surabaya. Indones.

FAO, 2000. The State of World Fisheries and Aquaculture Part 2: Selected Issues Facing Fishers and Aquaculturists, the State of World Fisheries and Aquaculture. Food & Agriculture Org.

Gammon, M.A., 2011. Optimization of fishing vessels using a multi-objective genetic algorithm. Ocean Eng 38, 1054–1064. https://doi.org/10.1016/j.oceaneng.2011.03.001.

Grigoropoulos, G.J., Loukakis, T.A., 1988. A new method for developing hull forms with superior seakeeping qualities. Proc. CADMO 88.

Guan, G., Wang, L., Geng, J., Zhuang, Z., Yang, Q., 2021. Parametric automatic optimal design of USV hull form with respect to wave resistance and seakeeping. Ocean Eng 235, 109462. https://doi.org/10.1016/j.oceaneng.2021.109462.

Hirt, C.W., Nichols, B.D., 1981. Volume of fluid (VOF) method for the dynamics of free boundaries. J. Comput. Phys. 39, 201–225.

Hüffmeier, J., Lundman, J., Elern, F., 2020. Trim and ballast optimization for a tnaker based on machine learning. Ecoprodigi, Intereg Balt. Sea Reg.

IMO, 2018. Initial IMO strategy on reduction of GHG emissions from ships. Resolut. MEPC 304 (72), 17, 72.

ITTC, 2014. Practical Guidelines for Ship Resistance CFD, 27th. ITTC – Recommended Procedures and Guidelines.

ITTC, 2008. Guidelines. Testing and extrapolation methods. High speed marine Vehicles resistance test. Recomm. Proced. Guidel. Test. Extrapolation methods, propulsion, performance, predict. powering margins 14–20.

Ittc, I., 2011. Practical guidelines for ship CFD applications. Recomm. Proced. Guidel. 18.

Jin, D., Thunberg, E., 2005. An analysis of fishing vessel accidents in fishing areas off the northeastern United States. Saf. Sci. 43, 523–540.

Lackenby, H., 1950. On the systematic geometrical variation of ship forms. Trans. TINA 92, 289–316.

Liu, S., Shang, B., Papanikolaou, A., 2019. On the resistance and speed loss of full type ships in a seaway. Sh. Technol. Res. 66, 161–179.

Mancini, S., 2015. The problem of verification and validation processes of CFD simulations of planing hulls. Dep. Ind. Eng. Univ. Degli Stud. Di Napoli.

Muzaferija, S., 1998. Computation of free surface flows using interface-tracking and interface-capturing methods. Nonlinear water-wave Interact. Comput. Mech. Southampt.

Obeng, F., Domeh, V., Khan, F., Bose, N., Sanli, E., 2022. Analyzing operational risk for small fishing vessels considering crew effectiveness. Ocean Eng 249, 110512.

Ozmen, G., 1995. Hull Form Optimisation of Fishing Vessels with Respect to Seakeeping. University of Glasgow, United Kingdom.

Pérez-Arribas, F., Silva-Campillo, A., D\'\iaz-Ojeda, H.R., 2022. Design of dihedral bows: a new type of developable added bulbous bows—experimental results. J. Mar. Sci. Eng. 10, 1691.

Reichel, M., Minchev, A., Larsen, N.L., 2014. Trim optimisation-theory and practice. TransNav Int. J. Mar. Navig. Saf. Sea Transp. 8.

Roache, P.J., 1998. Verification and Validation in Computational Science and Engineering. Hermosa, Albuquerque, NM.

Rotteveel, E., Hekkenberg, R., van der Ploeg, A., 2017. Inland ship stern optimization in shallow water. Ocean Eng 141, 555–569.

Roy, R., Hinduja, S., Teti, R., 2008. Recent advances in engineering design optimisation: Challenges and future trends. CIRP Ann 57, 697–715.

Shivachev, E., Khorasanchi, M., Day, S., Turan, O., 2020. Impact of trim on added resistance of KRISO container ship (KCS) in head waves: an experimental and numerical study. Ocean Eng 211, 107594.

Simonsen, C.D., Otzen, J.F., Joncquez, S., Stern, F., 2013. EFD and CFD for KCS heaving and pitching in regular head waves. J. Mar. Sci. Technol. 18, 435–459.

Terziev, M., Tezdogan, T., Incecik, A., 2022. Scale effects and full-scale ship hydrodynamics: a review. Ocean Eng 245, 110496. https://doi.org/10.1016/j.oceaneng.2021.110496.

Tran, T.G., Nguyen, H.V., Huynh, Q. Van, 2023. A method for optimizing the hull form of fishing vessels. J. Sh. Res. 67, 72–91.

Ugurlu, F., Yildiz, S., Boran, M., Ugurlu, Ö., Wang, J., 2020. Analysis of fishing vessel accidents with Bayesian network and Chi-square methods. Ocean Eng. 198, 106956.

Wang, J., Pillay, A., Kwon, Y.S., Wall, A.D., Loughran, C.G., 2005. An analysis of fishing vessel accidents. Accid. Anal. Prev. 37, 1019–1024.

Wen, P., Fadillah, A., 2022. The effect of trim on stability and seakeeping of tanker, container, and bulk carrier. IOP Conf. Ser. Earth Environ. Sci., 12037

Xiaobo, Z., 2017. Comparison of response surface method and Kriging method for approximation modeling. In: 2017 2nd International Conference on Power and Renewable Energy (ICPRE), pp. 66–70.

Yulianti, S., Samuel, S., Nainggolan, T.S., Iqbal, M., 2022. Meshing generation strategy for prediction of ship resistance using CFD approach. IOP Conf. Ser. Earth Environ. Sci. 1081, 012027. https://doi.org/10.1088/1755-1315/1081/1/012027.

Zhang, S., Tezdogan, T., Zhang, B., Xu, L., Lai, Y., 2018. Hull form optimisation in waves based on CFD technique. Ships Offshore Struct. 13, 149–164. https://doi.org/10.1080/17445302.2017.1347231.

Zhao, C., Wang, W., Jia, P., Xie, Y., 2021. Optimisation of hull form of ocean-going trawler. Brodogr. An Int. J. Nav. Archit. Ocean Eng. Res. Dev. 72, 33–46.